Richtmyer - Meshkov instability in a spherical target with density variation

Labakanta Mandal *, Sourav Roy, Rahul Banerjee, Manoranjan Khan and M.R.Gupta

Department of Instrumentation Science & Center for Plasma Studies

Jadavpur University, Kolkata-700032, India

E-mail: labakanta@gmail.com

Abstract.

The motion of unstable fluid interface due to Richtmyer - Meshkov (RM) instability incorporating with density variation has been studied in a spherical target using Lagrangian formulation. During the compression in Inertial Confinement Fusion (ICF) process, the density of deuterium - tritium (DT) fuel increases 1000 times greater than the density of gaseous DT fuel within the core of spherical target. We have extended the feature of density variation [PRA,84-Mikaelian & Lindl] in spherical geometry. Due to convergent shock impingement, the perturbed interface will be nonspherical which leads to the density variation in both radial as well as in polar angle. We have shown that the interface of perturbed surface decreases with time to reach a

minimum and then kick back to gradual increase. As the perturbed radius decreases, the density increases and reaches a maxima corresponding to a minima of perturbed radius. This is the practical situation of density characteristics during implosion of ICF. The numerical results based on our analytical work show a good qualitative agreement with some experimental as well as simulation results.

---

1. Introduction

The direct driven Inertial Confinement Fusion (ICF) process can be divided into four stages, i.e., the laser radiation, the implosion-compression, the fusion ignition and the deuterium-tritium (DT) fuel burn. Mainly, in the second stage, the hydrodynamical interfacial fluid instabilities can act. The Rayleigh-Taylor (RT) instability can occur during the two phases of the ablative acceleration and the compression deceleration of the ICF implosion. In addition to RT instability, RM instability can occur when shocks pass through the irregular fluid interface. The nonspherical implosion in ICF process generates the shear flow causing the Kelvin-Helmholtz (KH) instability. **The growth of these instability can be affected by the density ratio of two fluids, geometry of the interface, compressibility effects, heat conduction and mass flow at the interface**. These instabilities should be mitigated for efficient compression in ICF experiment.

Mikaelian and Lindl[1] explained that the smooth density gradient at the interface stabilize the hydrodynamic instability in ICF situation. However, they considered a constant and exponential density gradient at the interface. Initially this work started by Plesset [2] for stability condition of underwater explosion considering the velocity along the radial direction only. He discussed the stability and instability conditions depending on the pressure difference at the interface of bubble. Growth of perturbed interface due to density [3]−[4] variation has been discussed in different geometry [5]. RT growth stabilization effect has been showed very well by hot spot dynamics [6] − [10] in ablation situation of ICF. However, Ramshaw [11] extended Mikaelian's[12], [13] work using Lagrangian formulation in hydrodynamical model in a spherical geometry. In this context, several authors [14] − [18] pointed out that during implosion(acceleration phase) the fluid is compressed hence the fluid density increases rapidly inside the sphere. Similarly, during the blow off(deceleration phase) the fluid is relaxed to expand and fluid density falls exponentially from the perturbation surface. During robustness compression [19] − [21] of direct driven ICF target, the density can be compressed by 100 to 200 times of liquid DT density at cryogenic temperature [22] − [23]. Perturbation amplitudes and its growth rates of hydrodynamical instabilities of laser fusion targets has been studied in acceleration and deceleration phase including the heat conduction effect [24] − [25]using Lagrangian formulation. Numerical,simulation and experimental results[26] − [29] of RMI are performed in cylindrical geometry considering implosion and explosion situation. However, the growth of RM instability can be suppressed due

to different shape of the interface [30] − [31]. Recently, X-ray and proton radiography technique has been used to study the fast ignition implosion in cylindrical geometry [32] − [34]. The simulation result well agree with the experimental result. So, density variation and sphericity are two key factor to understand clearly for successful of ICF process.

In this paper, we investigate the nonlinear evolution of perturbed interface in spherical geometry considering mean interface $[R(t)]$ and angular amplitude both are dynamical variables. As a result, the growth and growth rate of nonspherical interface due to implosion has been changed for both variable with time. Hence, the nonspherical irregular interface changes explicitly with radius, polar angle and time. Analytically and numerically we have shown the density variation for compression-blow off situation of ICF. Theoretically high compression may be achieved depending on the density variation at the interface of two fluids. Polar plot also shows the time evolution of the interface in spherical geometry. Growth reduction has been shown for high value of mode number for a particular initial conditions.

The paper is organized as follows: section 2, deals with basic assumptions and equation of continuity. Expressions of kinetic energy of two fluids followed by Lagrangian equation of motion have been discussed in section 3. The nonlinear equations which describe the growth and the growth rate of perturbed interface are presented in section 4. Section 5 contains results and discussions. Finally, we conclude the results with a hope of future study on this work.

2. Basic equation

We have considered two concentric spherical shells having two incompressible, immiscible and inviscid fluids of density ρ_1 and ρ_2. The unperturbed interface at any time is given by $r = R(t)$. The lighter fluid is bounded in the inner shell at $R_1 < \hat{r} < R(t)$ and the heavier fluid is ceiling at radius R_2, where, $R_1 \ll R(t) \ll R_2$, as shown in Fig.1. Here we assume that the interface is perturbed to $r = \hat{r}$ which is given by

$$\hat{r}(t,\theta) = \hat{R}(t) + \sqrt{\frac{2l+1}{2}} a_l(t) P_l(cos\theta)$$
$$\hat{r}(t,\theta) = \left[\hat{R}(t) + \delta R_{a_l}\right] + \sqrt{\frac{2l+1}{2}} a_l(t) P_l(cos\theta) \quad (1)$$

where, $a_l \ll R$ and $\hat{R}, a_l, P_l(cos\theta)$ are mean radius of perturbed interface, angular displacement and Legendre polynomial of mode number l respectively and $\delta R_{a_l} = R[1 - (\frac{a_l}{R})^2]$. Here we ignore the azimuthal dependence of perturbed interface due to spherical symmetry. However, simulation [35] study shows that there is a weak dependence of growth rate on azimuthal angle.

Now we assume that the fluid motion is irrotational in the interface region,i.e., its obey Laplace's equation $\nabla^2\Phi = 0$. So the velocity potentials for lighter and heavier fluids are

$$\Phi_1 = -\frac{R^2\dot{R}}{r} + \frac{1}{l}\sqrt{\frac{2l+1}{2}}\left(R\dot{a_l} + 2\dot{R}a_l\right)\left(\frac{r}{R}\right)^l P_l(cos\theta) \quad (2)$$

$$\Phi_2 = -\frac{R^2\dot{R}}{r} - \frac{1}{l+1}\sqrt{\frac{2l+1}{2}}\left(R\dot{a_l} + 2\dot{R}a_l\right)\left(\frac{R}{r}\right)^{l+1} P_l(cos\theta) \quad (3)$$

respectively.

Due to shock impingement, the nonspherical perturbed interface leads to the density

variation as follows

$$\rho_1(r,\theta,t) = \rho_1 + \rho_{11}(r,t)P_l(cos\theta); \qquad R_1 < r < \hat{r} \tag{4}$$

$$\rho_2(r,\theta,t) = \rho_2 + \rho_{21}(r,t)P_l(cos\theta); \qquad \hat{r} < r \leq R_2 \tag{5}$$

for lighter and heavier fluid, respectively. This type of density variation feature was not considered in previous studies.

2.1. Equation of continuity

The equation of continuity in spherical polar coordinate can be written as

$$\frac{\partial \rho}{\partial t} + u_{1r}\frac{\partial \rho}{\partial r} + \frac{u_{1\theta}}{r}\frac{\partial \rho}{\partial t} = 0 \tag{6}$$

where, $u_{1r} = \frac{\partial \Phi}{\partial r}$ and $u_{1\theta} = \frac{1}{r}\frac{\partial \Phi}{\partial \theta}$ are radial and transverse component of fluid velocity, respectively. Substituting the value of $u_{1r}, u_{1\theta}$and ρ_1, we get the following equation for lighter fluid

$$\frac{\partial \rho_{11}}{\partial t} + \left[\frac{R^2\dot{R}}{r^2} + \sqrt{\frac{2l+1}{2}}\left(R\dot{a_l} + 2\dot{R}a_l\right)\left(\frac{r^{(l-1)}}{R^l}\right)P_l(cos\theta)\right]\frac{\partial \rho_{11}}{\partial r}$$
$$+\frac{1}{l}\sqrt{\frac{2l+1}{2}}\left(R\dot{a_l} + 2\dot{R}a_l\right)\left(\frac{r^{(l-1)}}{R^l}\right)\frac{dP_l}{d\theta}(cos\theta) = 0 \tag{7}$$

Neglecting the product term $(a_l \times \rho_{11})$, we get the following partial differential equation

$$\frac{\partial \rho_{11}}{\partial t} + \frac{R^2\dot{R}}{r^2}\frac{\partial \rho_{11}}{\partial r} = 0 \tag{8}$$

The solution of the above p.d.e is given by,

$$\rho_{11}(r,t) = \rho_{11}e^{\frac{\mu}{3}\left[R^3(t) - r^3\right]} \tag{9}$$

Similarly, we get the density variation for heavier fluid as follows

$$\rho_{21}(r,t) = \rho_{21}e^{\frac{\mu}{3}\left[R^3(t) - r^3\right]} \tag{10}$$

where, μ is a positive constant for implosion situation.

The mass conservation at the interface gives us the following relation

$$\frac{\rho_{11}}{\rho_1} = \frac{\rho_{21}}{\rho_2} \tag{11}$$

3. Kinetic energy

To study the equation of motion of perturbed interface we have calculated the kinetic energy of the two fluids.

3.1. Kinetic energy of lighter fluid

The kinetic energy of lighter fluid can be calculated in the following way

$$\begin{aligned}
T_1 &= \frac{1}{2}\int d\Omega \int_{R_1}^{\hat{r}} \rho_1(r,\theta,t)\Big[|\nabla\Phi_1|^2\Big] r^2 dr \\
&= \frac{1}{2}\int d\Omega \int_{R_1}^{\hat{r}} \Big[\rho_1 + \rho_{11}(r,t)P_l(cos\theta)\Big]\left[\left(\frac{\partial\Phi_1}{\partial r}\right)^2 + \frac{1}{r^2}\left(\frac{\partial\Phi_1}{\partial\theta}\right)^2\right] r^2 dr \\
&= \frac{1}{2}\int d\Omega \int_{R_1}^{\hat{r}} \Big[\rho_1 + \rho_{11}(r,t)P_l(cos\theta)\Big]\left[\frac{R^4\dot{R}^2}{r^4} + 2\frac{R^2\dot{R}}{r^2}\sqrt{\frac{2l+1}{2}}\left(R\dot{a}_l + 2\dot{R}a_l\right)\left(\frac{r^{(l-1)}}{R^l}\right)P_l(cos\theta)\right. \\
&\left. + \left(\frac{2l+1}{2}\right)\left(R\dot{a}_l + 2\dot{R}a_l\right)^2\left(\frac{r^{2(l-1)}}{R^{2l}}\right)\Big(P_l(cos\theta)\Big)^2 + \frac{1}{l^2}\left(\frac{2l+1}{2}\right)\left(R\dot{a}_l + 2\dot{R}a_l\right)^2\left(\frac{r^{2(l-1)}}{R^{2l}}\right)\left(\frac{dP_l}{d\theta}\right)^2\right] r^2 dr \\
&= T_{10} + T_{1r\theta}
\end{aligned} \tag{12}$$

Where, T_{10} and $T_{1r\theta}$ are the kinetic energy coming from homogeneous density ρ_1 and inhomogeneous density $\rho_{11}(r,t)$ part of the lighter fluid, respectively. Now using Eq. 9, we get $T_{1r\theta}$ as follows,

$$\begin{aligned}
T_{1r\theta} = \frac{\rho_{11}}{2}\int P_l(cos\theta)d\Omega \int_{R_1}^{\hat{r}} &\left[\frac{R^4\dot{R}^2}{r^2} + 2R^2\dot{R}\sqrt{\frac{2l+1}{2}}\left(R\dot{a}_l + 2\dot{R}a_l\right)\left(\frac{r^{(l-1)}}{R^l}\right)P_l(cos\theta)\right. \\
&\left. + \left(\frac{2l+1}{2}\right)\left(R\dot{a}_l + 2\dot{R}a_l\right)^2\left(\frac{r}{R}\right)^{2l}\Big(P_l(cos\theta)\Big)^2\right.
\end{aligned}$$

$$+\frac{1}{l^2}\left(\frac{2l+1}{2}\right)\left(R\dot{a}_l+2\dot{R}a_l\right)^2\left(\frac{r}{R}\right)^{2l}\left(\frac{dP_l}{d\theta}\right)^2\Bigg]e^{\frac{\mu}{3}\left[R^3(t)-r^3\right]}dr \quad (13)$$

Similarly, we have calculated the kinetic energy for heavier fluid in the preceding section.

3.2. Kinetic energy of heavier fluid

$$T_2=\frac{1}{2}\int d\Omega\int_{\hat{r}}^{R_2}\rho_2(r,\theta,t)\Big[|\nabla\Phi_2|^2\Big]r^2dr$$

$$=\frac{1}{2}\int d\Omega\int_{\hat{r}}^{R_2}\Big[\rho_2+\rho_{21}(r,t)P_l(cos\theta)\Big]\left[\left(\frac{\partial\Phi_2}{\partial r}\right)^2+\frac{1}{r^2}\left(\frac{\partial\Phi_2}{\partial\theta}\right)^2\right]r^2dr$$

$$=\frac{1}{2}\int d\Omega\int_{\hat{r}}^{R_2}\Big[\rho_2+\rho_{21}(r,t)P_l(cos\theta)\Big]\Bigg[\frac{R^4\dot{R}^2}{r^4}+2\frac{R^2\dot{R}}{r^2}\sqrt{\frac{2l+1}{2}}\left(R\dot{a}_l+2\dot{R}a_l\right)\left(\frac{R^{(l+1)}}{r^{(l+2)}}\right)P_l(cos\theta)$$

$$+\left(\frac{2l+1}{2}\right)\left(R\dot{a}_l+2\dot{R}a_l\right)^2\left(\frac{R^{2(l+1)}}{r^{2(l+2)}}\right)\left(P_l(cos\theta)\right)^2$$

$$+\frac{1}{(l+1)^2}\left(\frac{2l+1}{2}\right)\left(R\dot{a}_l+2\dot{R}a_l\right)^2\left(\frac{R^{2(l+1)}}{r^{2(l+2)}}\right)\left(\frac{dP_l}{d\theta}\right)^2\Bigg]r^2dr$$

$$=T_{20}+T_{2r\theta} \quad (14)$$

Where, T_{20} and $T_{2r\theta}$ are the kinetic energy coming from homogeneous density ρ_2 and inhomogeneous density $\rho_{21}(r,t)$ part of the lighter fluid, respectively, and $\int d\Omega = 2\pi\int\sin\theta d\theta$=solid angle. Now using Eq. 10, we get $T_{2r\theta}$ as follows,

$$T_{2r\theta}=\frac{\rho_{21}}{2}\int d\Omega\int_{\hat{r}}^{R_2}\Bigg[\frac{R^4\dot{R}^2}{r^4}+2\frac{R^2\dot{R}}{r^2}\sqrt{\frac{2l+1}{2}}\left(R\dot{a}_l+2\dot{R}a_l\right)\left(\frac{R^{(l+1)}}{r^{(l+2)}}\right)P_l(cos\theta)$$

$$+\left(\frac{2l+1}{2}\right)\left(R\dot{a}_l+2\dot{R}a_l\right)^2\left(\frac{R^{2(l+1)}}{r^{2(l+2)}}\right)\left(P_l(cos\theta)\right)^2$$

$$+\frac{1}{(l+1)^2}\left(\frac{2l+1}{2}\right)\left(R\dot{a}_l+2\dot{R}a_l\right)^2\left(\frac{R^{2(l+1)}}{r^{2(l+2)}}\right)\left(\frac{dP_l}{d\theta}\right)^2\Bigg]e^{\frac{\mu}{3}\left[R^3(t)-r^3\right]}r^2dr \quad (15)$$

3.3. Lagrangian equation of motion

Now we have formulated the problem using Lagrangian equation of motion. The present problem is related to the RM instability i.e., shock impingement at the interface of two

fluid and hence neglected the potential energy. So, we have Lagrangian equation of motion as follows

$$\frac{d}{dt}\left(\frac{\partial T}{\partial \dot{q}}\right) - \frac{\partial T}{\partial q} = 0 \tag{16}$$

where, $T = T_{1r\theta} + T_{2r\theta}$ and $q \to \mathrm{R}$ and a_l both are dynamical vriable.

4. Nonlinear equation

Using eqs.13 & 15, We get from eq. 16, a pair of coupled nonlinear second order following differential equation. The detailed calculations are given in appendix.

$$f_{1R}(R,a_l)\ddot{R} + f_{2R}(R,a_l)\ddot{a_l} + f_{3R}(R,a_l)\dot{R}^2 + f_{4R}(R,a_l)(\dot{a_l})^2 + f_{5R}(R,a_l)\dot{R}\dot{a_l} = 0 \tag{17}$$

$$f_{1a_l}(R,a_l)\ddot{R} + f_{2a_l}(R,a_l)\ddot{a_l} + f_{3a_l}(R,a_l)\dot{R}^2 + f_{4a_l}(R,a_l)(\dot{a_l})^2 + f_{5a_l}(R,a_l)\dot{R}\dot{a_l} = 0 \tag{18}$$

From this two second order nonlinear differential equation we get following four first order differential equation, which describes the growth and growth rate of perturbed interface.

$$\frac{dX_1}{d\tau} = X_3 \tag{19}$$

$$\frac{dX_2}{d\tau} = X_4 \tag{20}$$

$$\frac{dX_3}{d\tau} = \frac{n_1 d_2 - n_2 d_1}{m_1 n_2 - m_2 n_1} \tag{21}$$

$$\frac{dX_4}{d\tau} = \frac{m_2 d_1 - m_1 d_2}{m_1 n_2 - m_2 n_1} \tag{22}$$

where, $X_1 = \frac{R}{R_2}, X_2 = \frac{a_l}{R_2}$ $m_1 = \xi_1(X_1, X_2), m_2 = \xi_2(X_1, X_2), n_1 = \xi_3(X_1, X_2)$ and $n_2 = \xi_1(X_1, X_2)$ are nondimensional perturbed radial displacement, angular displacement, radial velocity and angular velocity respectively.

5. Results & Discussions

The feasible analytical solution of this set of equations is quite impossible. We can numerically solve this set of equations using Runge-Kutta-Fehlberg numerical technique. The numerical results shows that due to the shock impingement, the interface decreases and consequently the DT fuel fuel is compressed during acceleration phase with time. The perturbed interface attains a minimum position and then kicks back to gradually increasing in time (Fig.2a) during the deceleration phase. The density increases as the perturbed interface decreases and attains a maximum density corresponding to minimum of perturbed interface then the density gradually decreases (blow-off situation) as the perturbed radius increases again(Fig.2e). This is the practical situation of compression-blow off process of ICF. During acceleration phase the fuel compression is maximum. The dotted line which also represents the growth of interface with time when $\alpha = \mu R_2^3 = 0$. However,dash-dot (blue) and solid (red) line for $\alpha = 10$ and 15 respectively, represents the stabilization due to density variation. Our this analytical results show a qualitative good agreement with simulation[7] as well as experimental results[32], [33], [34]. Though the experiment has been done in cylindrical geometry, the radius of a cylinder can be equivalently represented by the radius of a sphere. We have also shown the polar plot of perturbed surface at different time (Fig.3,4,5). We have considered the density ratio $r = 10, l = 50$(Legendre polynomial mode number) for numerical calculation. This type of density ratio[13] is appropriate for ICF process. We have shown in Fig.6 that the growth rate is maximum at $l = 50$.

6. Conclusion & future scope

Maximum compression can be achieved depending on the density variation at the interface. The acceleration and deceleration phase can be better understood from the numerical results. However, in this work we do not consider the temperature effect which is more realistic. In future we can take attempt to include the temperature effect also.

7. Acknowledgment

This work is supported by the Department of Science & Technology, Government of India under grant no. SR/S2/HEP-007/2008.

Appendix

The details of calculation for kinetic energy is given below.

$$T_{1r\theta} = \frac{\rho_{11}}{2}\int P_l(cos\theta)d\Omega \int_{R_1}^{\hat{r}} \left[\frac{R^4\dot{R}^2}{r^2} + 2R^2\dot{R}\sqrt{\frac{2l+1}{2}}\left(R\dot{a_l} + 2\dot{R}a_l\right)\left(\frac{r^{(l-1)}}{R^l}\right)P_l(cos\theta)\right.$$
$$+\left(\frac{2l+1}{2}\right)\left(R\dot{a_l} + 2\dot{R}a_l\right)^2\left(\frac{r}{R}\right)^{2l}\left(P_l(cos\theta)\right)^2$$
$$\left.+\frac{1}{l^2}\left(\frac{2l+1}{2}\right)\left(R\dot{a_l} + 2\dot{R}a_l\right)^2\left(\frac{r}{R}\right)^{2l}\left(\frac{dP_l}{d\theta}\right)^2\right]e^{\frac{\mu}{3}\left[R^3(t)-r^3\right]}dr \tag{23}$$

$$= \frac{\rho_{11}}{2}\int d\Omega \int_{R_1}^{\hat{r}} \left[\frac{R^4\dot{R}^2}{r^2}P_l + 2R^2\dot{R}\sqrt{\frac{2l+1}{2}}\left(R\dot{a_l} + 2\dot{R}a_l\right)\left(\frac{r^{(l-1)}}{R^l}\right)(P_l)^2\right.$$
$$\left.+\left(\frac{2l+1}{2}\right)\left(R\dot{a_l} + 2\dot{R}a_l\right)^2\left(\frac{r}{R}\right)^{2l}(P_l)^3 + \frac{1}{l^2}\left(\frac{2l+1}{2}\right)\left(R\dot{a_l} + 2\dot{R}a_l\right)^2\left(\frac{r}{R}\right)^{2l}P_l\left(\frac{dP_l}{d\theta}\right)^2\right]e^{\frac{\mu}{3}\left[R^3(t)-r^3\right]}dr$$
$$= T_{1P_1} + T_{1P_2} + T_{1P_3} + T_{1P_\theta} \tag{24}$$

Where,

$$T_{1P_1} = \frac{R^4\dot{R}^2}{2}\rho_{11}\int P_l d\Omega \int_{R_1}^{\hat{r}} \frac{1}{r^2}e^{\frac{\mu}{3}\left[R^3(t)-r^3\right]}dr \tag{25}$$

$$T_{1P_2} = \frac{\rho_{11}}{2}\int d\Omega \int_{R_1}^{\hat{r}} \left[2R^2\dot{R}\sqrt{\frac{2l+1}{2}}\left(R\dot{a_l}+2\dot{R}a_l\right)\left(\frac{r^{(l-1)}}{R^l}\right)(P_l)^2\right] e^{\frac{\mu}{3}\left[R^3(t)-r^3\right]}dr \tag{26}$$

$$T_{1P_3} = \frac{\rho_{11}}{2}\int d\Omega \int_{R_1}^{\hat{r}} \left[\left(\frac{2l+1}{2}\right)\left(R\dot{a_l}+2\dot{R}a_l\right)^2\left(\frac{r}{R}\right)^{2l}(P_l)^3\right] e^{\frac{\mu}{3}\left[R^3(t)-r^3\right]}dr \tag{27}$$

$$T_{1P_\theta} = \frac{\rho_{11}}{2}\int d\Omega \int_{R_1}^{\hat{r}} \left[\frac{1}{l^2}\left(\frac{2l+1}{2}\right)\left(R\dot{a_l}+2\dot{R}a_l\right)^2\left(\frac{r}{R}\right)^{2l}P_l\left(\frac{dP_l}{d\theta}\right)^2\right] e^{\frac{\mu}{3}\left[R^3(t)-r^3\right]}dr \tag{28}$$

After a straight forward calculation of Eq. (25) and putting the value of $\hat{r}$ and expanding it upto second order of $(\frac{a_l}{R})$, we get the following equation

$$T_{1P_1} = 4\pi R^3\rho_1\Big(\frac{\rho_{11}}{\rho_1}\Big)\Big(\frac{\dot{R}^2}{2}\Big)\left[\frac{(a_l/R)}{\sqrt{2(2l+1)}}\Big(1+\mu R^3\Big)-\frac{(a_l/R)^2}{2}\Big(1+\frac{\mu R^3}{2}\Big)Q_l\right] \tag{29}$$

Similarly,

$$\begin{aligned} T_{1P_2} = 4\pi R^3\rho_1\Big(\frac{\rho_{11}}{\rho_1}\Big)\Big(\frac{\dot{R}^2}{R}\Big)\Big(R\dot{a_l}+2\dot{R}a_l\Big)\sqrt{\frac{2l+1}{2}}\Bigg[&\frac{(l+3+\mu R^3)}{l(2l+1)(l+3)}+\frac{(a_l/R)}{\sqrt{2(2l+1)}}Q_l \\ &+\left\{\Big(l-1-\mu R^3\Big)\frac{S_l}{4}-\frac{1}{2(2l+1)}\right\}\Big(\frac{a_l}{R}\Big)^2\Bigg] \end{aligned} \tag{30}$$

$$\begin{aligned} T_{1P_3} = 4\pi R^3\rho_1\Big(\frac{\rho_{11}}{\rho_1}\Big)\left(\frac{2l+1}{4}\right)\left(\frac{R\dot{a_l}+2\dot{R}a_l}{R}\right)^2\Bigg[&\left(1-\frac{\mu R^3}{2(l+2)}\right)\frac{Q_l}{(2l+1)^2} \\ &+\frac{\Big(a_l/R\Big)}{\sqrt{2(2l+1)}}S_l+\left\{\Big(l-\frac{\mu R^3}{2}\Big)\frac{X_l}{2}-\frac{1}{(2l+1)}\frac{Q_l}{2}\right\}\left(\frac{a_l}{R}\right)^2\Bigg] \end{aligned} \tag{31}$$

$$\begin{aligned} T_{1P_\theta} = 4\pi R^3\rho_1\Big(\frac{\rho_{11}}{\rho_1}\Big)\Big(2l+1\Big)\left(\frac{R\dot{a_l}+2\dot{R}a_l}{2lR}\right)^2\Bigg[&\frac{l(l+1)}{(2l+1)^2(l+2)}\Big(l+2+\frac{\mu R^3}{2}\Big)T_l \\ &+\frac{l(l+1)}{\sqrt{2(2l+1)}}\Big(\frac{a_l}{R}\Big)U_l+\left\{\frac{1}{2}\Big(l-\frac{\mu R^3}{2}\Big)V_l-\frac{1}{2(2l+1)}T_l\right\}l(l+1)\Big(\frac{a_l}{R}\Big)^2\Bigg] \end{aligned} \tag{32}$$

$$\begin{aligned} T_{2r\theta} = \frac{\rho_{21}}{2}\int d\Omega \int_{\hat{r}}^{R_2} \Bigg[&\frac{R^4\dot{R}^2}{r^4}+2R^2\dot{R}\sqrt{\frac{2l+1}{2}}\left(R\dot{a_l}+2\dot{R}a_l\right)\left(\frac{R^{(l+1)}}{r^{(l+4)}}\right)\left(P_l\right) \\ &+\left(\frac{2l+1}{2}\right)\left(R\dot{a_l}+2\dot{R}a_l\right)^2\left(\frac{R^{2(l+1)}}{r^{2(l+2)}}\right)\left(P_l\right)^2 \\ &+\frac{1}{(l+1)^2}\left(\frac{2l+1}{2}\right)\left(R\dot{a_l}+2\dot{R}a_l\right)^2\left(\frac{R^{2(l+1)}}{r^{2(l+2)}}\right)\left(\frac{dP_l}{d\theta}\right)^2\Bigg] e^{\frac{\mu}{3}\left[R^3(t)-r^3\right]}r^2dr \end{aligned} \tag{33}$$

$$= T_{2P_1}+T_{2P_2}+T_{2P_3}+T_{2P_\theta} \tag{34}$$

Where,

$$T_{2P_\theta} = 4\pi R^3 \rho_2 \Big(\frac{\rho_{21}}{\rho_2}\Big)\left(\frac{\dot{R}}{2}\right)^2 \left[\Big(1+\frac{\mu R^3}{2}\Big)\frac{(a_l/R)^2}{2}Q_l - \frac{(a_l/R)}{\sqrt{2(l+1)}}\Big(1+\mu R^3\Big)\right]$$

8. References

[1] Karning O Miakaelian and Lindl J D 1984 *Phys. Rev. A* **29** 290.

[2] Plesset M S 1954 *Jou. Appl. Phys.* **25** 96.

[3] Karning O Miakaelian 1983 *Phys. Rev. A* **28** 1637.

[4] Karning O Miakaelian 1986 *Phys. Rev. A* **33** 1216.

[5] Goncharov V N and Li D 2005 *Phys. Rev. E.* **71** 046306.

[6] Schiavi A and Atzeni S 2007 *Phys. Plasmas* **14** 070701.

[7] Sanz J *et al* 2005 *Phys. Plasmas* **12** 112702.

[8] Azechi H *et al* 2004 *Plasma Phys. Control Fusion* **46** B245.

[9] Azechi H *et al* 2004 *Plasma Phys. Control Fusion* **46** B245.

[10] Garnier J and Cherfils C 2005 *Phys. Plasmas* **12** 012704.

[11] Ramshaw J D 1999 *Phys. Rev. E* **60** 1775.

[12] Karning O Miakaelian 1990 *Phys. Rev. Lett.* **65** 992.

[13] Karning O Miakaelian 1990 *Phys.Rev. A* **42** 3400.

[14] Shiau J N, Goldman E B and Weng C I 1974 *Phy.Rev.Lett.* **32** 352.

[15] Henderson D B and Morse R L 1974 *Phys.Rev. Lett.* **32** 355.

[16] Bodner E. Stephen 1974 *Phys.Rev. Lett.* **33** 761.

[17] Cambell P M, Charatis G and Montry G R 1975 *Phy.Rev.Lett.* **34** 74.

[18] Petrasso R D et al 1996 *Phys.Rev. Lett.* **77** 2718.

[19] Ribeyre X, Schurtz G, Lafon M, Garela S and Weber S 2009 *Plasma Phys. Control Fusion* **51** 015013.

[20] Hallo L *et al* 2009 *Plasma Phys. Control Fusion* **51** 014001.

[21] Atzeni S, Schiavi and Marocchino A 2011 *Plasma Phys. Control Fusion* **53** 035010.

[22] McCrory R L *et al* 1988 *Nature* **335** 225.

[23] McCrory R L*et al* 1988 *Plasma Phys. Control Fusion* **31** 1517.

[24] Atzeni S *et al* 1986 *Comp. Phys. Communications* **43** 107.

[25] Temporal M, Jouen S, Masse L and Canaud B 2006 *Phys. Plasmas* **13** 122701.

[26] Zhang Q and Graham M J 1998 *Phys. Fluids* **10** 974.

[27] Mikaelian O Karning 2005 *Phys. Fluids* **17** 094105.

[28] Hosseini R H S and Takayama K 2005 *Phys. Fluids* **17** 084101.

[29] Zheng J G, Lee T S and Winoto H S 2008 *Math. Comput. Simulation* **79** 749.

[30] Mikaelian O Karning 2005 *Phys. Fluids* **17** 034101.

[31] Gupta M R, Roy S,Sarkar S, Khan M, Pant H C and Shrivastaba M K 2007 *Laser Part. Beams* **25** 503.

[32] Volpe L *et al* 2011 *Plasma Phys. Control Fusion* **53** 032003.

[33] Vauzour B *et al* 2011 *Phys. Plasmas* **18** 043108.

[34] Volpe L *et al* 2011 *Phys. Plasmas* **18** 012704.

[35] Sakagami H, Nishihara K 1990 *Phys.Rev. Lett.* **65** 432.

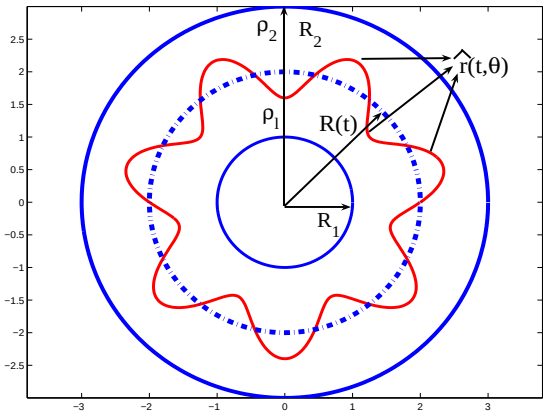

Figure 1. Geometry of the problem

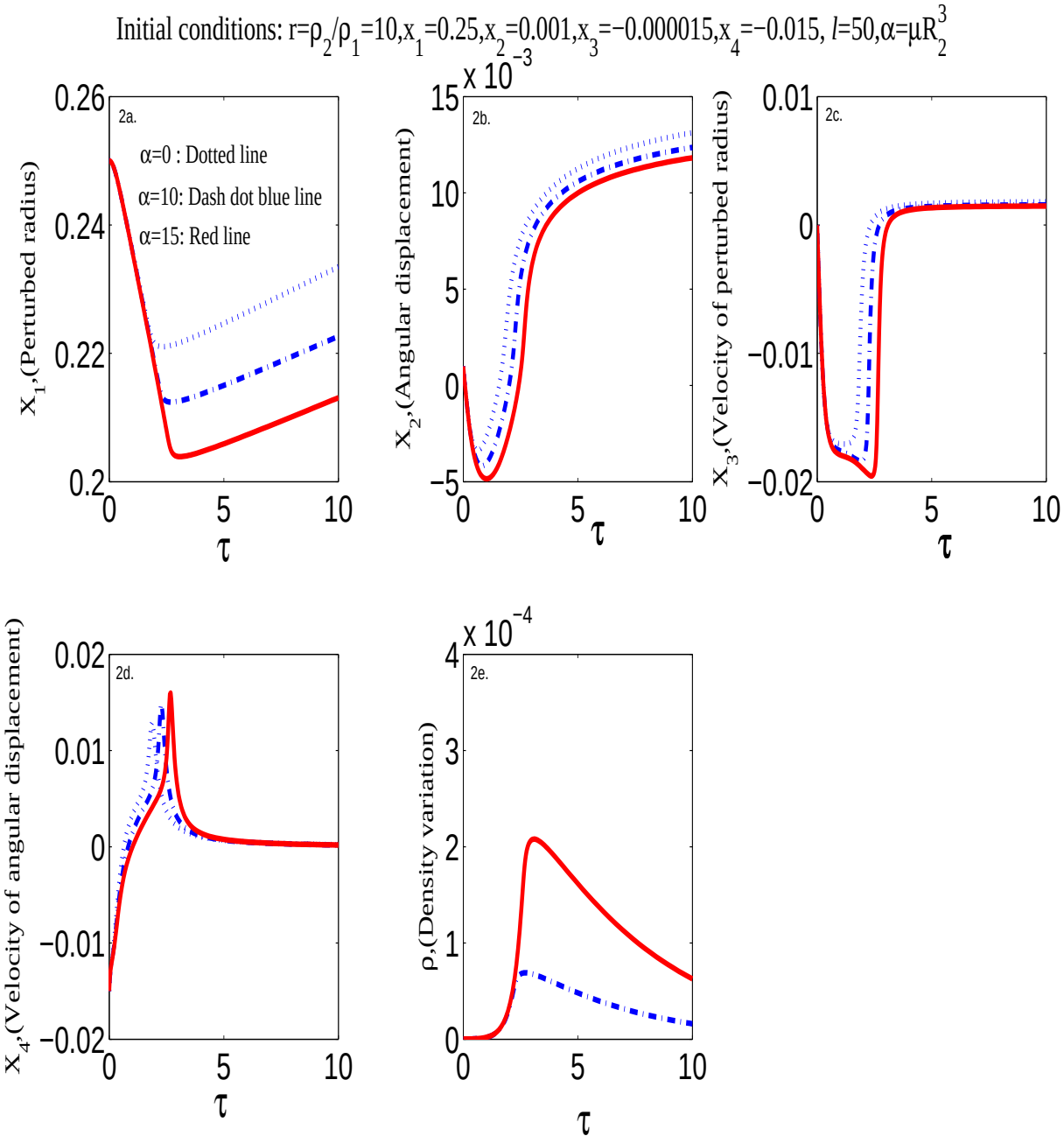
Initial conditions: r=ρ2/ρ1=10,x1=0.25,x2=0.001,x3=−0.000015,x4=−0.015, l=50,α=μR2^3
2a.
α=0 : Dotted line
α=10: Dash dot blue line
α=15: Red line
X1,(Perturbed radius)
2b.
x 10^−3
X2,(Angular displacement)
2c.
X3,(Velocity of perturbed radius)
2d.
X4,(Velocity of angular displacement)
2e.
x 10^−4
ρ,(Density variation)
τ

Figure 2.

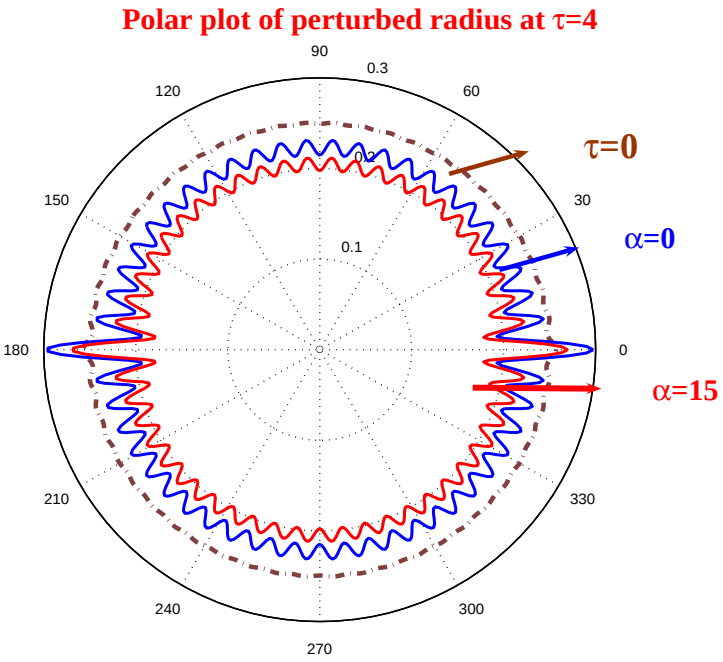
Polar plot of perturbed radius at τ=4
90
0.3
60
120
0.2
30
150
0.1
180
0
210
330
240
300
270
τ=0
α=0
α=15

Figure 3.

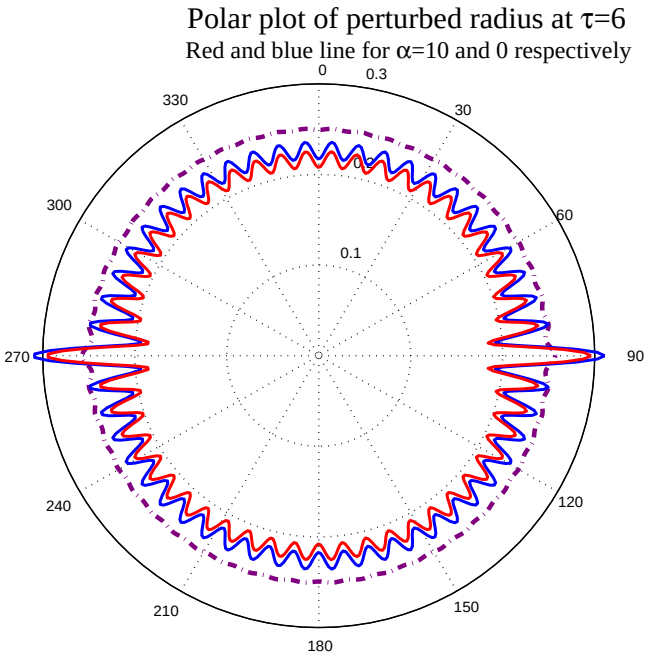
Polar plot of perturbed radius at τ=6
Red and blue line for α=10 and 0 respectively
0
0.3
30
60
90
120
150
180
210
240
270
300
330
0.1

Figure 4.

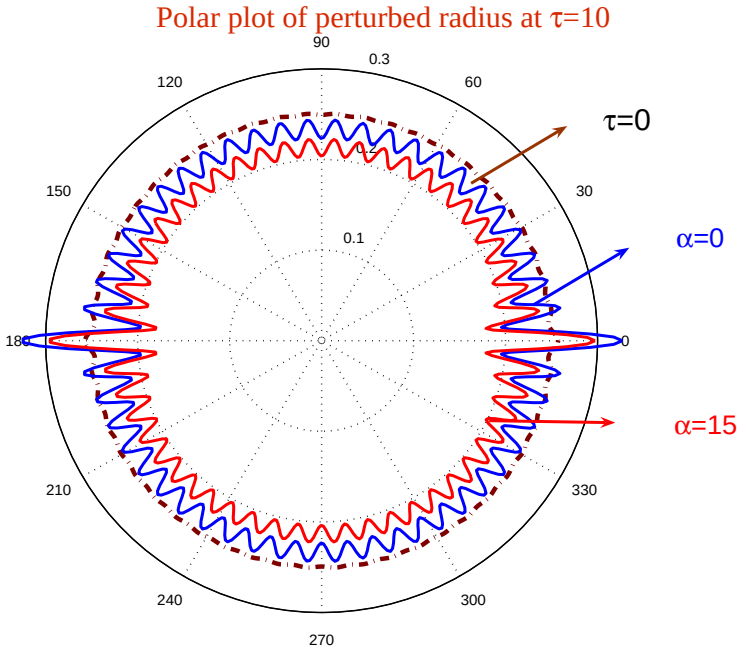
Polar plot of perturbed radius at τ=10
90
0.3
120
60
τ=0
0.2
150
30
α=0
0.1
180
0
α=15
210
330
240
300
270

Figure 5.

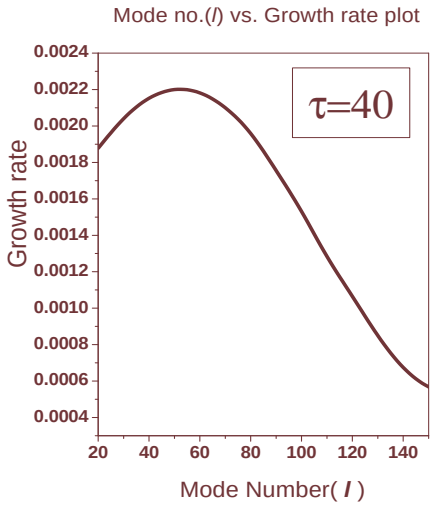
Mode no.(l) vs. Growth rate plot
τ=40
Growth rate
0.0024
0.0022
0.0020
0.0018
0.0016
0.0014
0.0012
0.0010
0.0008
0.0006
0.0004
20
40
60
80
100
120
140
Mode Number(l)

Figure 6.